Response to RC1: 'Comment on egusphere-2025-91 ' , Anonymous Referee #1, 11 Mar 2025

Review of Manuscript egusphere-2025-91 entitled '**Global validation of the Particulate Observing Scanning Polarimeter (POSP) Aerosol Optical Depth products over land**' by Zhe Ji, Zhengqiang Li, Gerrit de Leeuw, Zihan Zhang, Yan Ma, Zheng Shi, Cheng Fan, and Qian Yao

On behalf of all co-authors, we thank Referee #1 for the insightful and extensive comments which certainly contribute to the substantial improvement of the manuscript (MS). Below we respond to each of the general, major and specific comments which are copied below (in black). In addition to the numbered major and specific comments, we have numbered the general comments as GC1-GC5. After each comment we provide our response, in red, together with changes in the revised MS. Line numbers (indicated by L) mentioned by Referee #1 refer to the original MS as published in the AMT discussion Section and revisions are quoted with line numbers (indicated by LR) referring to the revised MS.

GC1: The specific data quality control procedures for POSP (e.g., cloud detection, outlier removal) remin unclear in the manuscript, potentially affecting result reproducibility. It is recommended to supplement detailed descriptions of POSP data preprocessing steps (e.g., cloud masking, pixel screening criteria) and clarify their impacts on the matching strategy.

Response to GC1: Thank you for pointing this out. We overlooked the description of the data preprocessing step, and we appreciate your reminder, which is very helpful in improving the quality of the manuscript. Since the algorithm proposed in this study is specifically designed for cloud-free land pixels, we removed land pixels that might contain clouds or ice/snow before retrieval. When retrieval pixels contain potential cloud contamination, the results tend to be significantly overestimated. A strict cloud detection process can effectively mitigate this issue. Additionally, to ensure the reliability of the validation, we adopted the following matching strategies:

"In this study, considering the 6.4 km spatial resolution of the POSP, the following strategies to match POSP and AERONET AOD data have been devised to ensure reliable AOD validation results while accounting for spatial consistency: satellite data are averaged over a window of 3 × 3 pixels centred on the AERONET site, and ground-based observations are averaged over 30 minutes before and after the time of the satellite overpass. To mitigate the uncertainty associated with averaging data, a minimum of two or more ground-based observations are required in the temporal matchup window, and the spatial-temporal matchup window must encompass more than three valid satellite pixels (Chu et al., 2002)." (LR 145-151)

A detailed description of the preprocessing has been added to the Methods section.

"As an optical sensor, POSP observations are inherently susceptible to cloud interference. To mitigate cloud contamination, it is essential to filter out cloud-affected pixels before retrieval. Given the single-angle observation method of POSP, this study adopts cloud detection strategies from MODIS, which have been extensively validated (Frey et al., 2008). Specifically, two methods are employed: the apparent reflectance threshold method and the apparent reflectance spatial variation detection method (Martins et al., 2002). The former effectively identifies optically thick clouds with high reflectance or substantial water vapor content, while the latter is particularly useful for detecting cloud edges, shadows, thin clouds, and dispersed cloud formations.

The land surface exhibits low reflectance in the blue band, whereas clouds have high reflectance.

Therefore, a pixel is identified as a cloud when its reflectance at the 443 nm band exceeds a certain threshold. The 1380 nm band lies within a strong water vapor absorption region, where the reflectances from land surfaces and low clouds are generally low. As a result, only high clouds, mostly above the heights where atmospheric water vapor is located, are visible in this band. Pixels with high reflectance at 1380 nm are therefore typically classified as high clouds. Furthermore, cloud edges typically exhibit high spatial variability due to mixed pixels and partial cloud coverage. The spatial variation characteristics of the 443 nm and 1380 nm bands can effectively identify cloud-edge pixels. The combination of their spatial differences helps reduce misclassification at cloud boundaries and improves the accuracy of cloud detection.

Surface conditions such as snow and water also affect the inversion. Since the retrieval algorithm is explicitly designed for clear-sky over non-ice land surfaces, pixels over water, ice, and snow must be excluded. The detection of water and snow pixels is achieved using the Normalized Difference Water Index (NDWI) and the Normalized Difference Snow/Ice Index (NDSI), respectively, with specific identification thresholds presented in Table 1.

$$NDWI = \frac{\rho_{670} - \rho_{865}}{\rho_{670} + \rho_{865}} \tag{9}$$

$$NDSI = \frac{\rho_{670} - \rho_{2250}}{\rho_{670} + \rho_{2250}} \tag{10}$$

While the aforementioned cloud detection strategy provides a foundation for minimizing cloud contamination, potential for further improvement remains. Given the relatively coarse spatial resolution of POSP (6.4 km) and its limited spectral coverage, certain pixels that contain residual clouds may remain undetected. The simulation analysis by Kassianov and Ovtchinnikov (2008) pointed out that multiple scattering of clouds can lead to overestimated AOD retrievals when the residual clouds are not fully screened. Sogacheva et al. (2017) further removed the cloud-contaminated pixels using a cloud post-processing scheme. To enhance cloud-mask accuracy, a dedicated cloud detection algorithm for POSP is still needed. We aim to further enhance the cloud detection algorithm in future work.

Table 1 Summary of screening thresholds.

Items	Purpose
$\rho_{443} < 0.02 \; or \; \rho_{443} > 0.4$	Cloud
$\sigma_{443} > 0.038$	Cloud
$\rho_{1380} > 0.02 \; and \; Height < 1500$	Cloud
$\sigma_{1380} > 0.005$	Cloud
$NDWI > 0$	Water
$NDSI > 0.4$	Snow/Ice

” (LR 185-213)

GC2:. Line24, Lines 178-182: The significant underestimation in high-AOD regions (e.g., North Africa) is attributed to "aerosol model errors" without specific analysis of discrepancies between model assumptions and actual aerosol characteristics. Further investigation into aerosol model classification and its impact on retrieval errors is suggested.

Response to GC2: We sincerely apologize for any misunderstanding caused by our oversight. First, Fig. 14 in the manuscript shows that:

"POSP AOD is slightly lower than MODIS DB AOD over North Africa and the Arabian Peninsula, while it is much closer to MODIS MAIAC AOD in these regions. Overall, POSP AOD shows similar features as MAIAC AOD over North Africa and the Arabian Peninsula, while it is more consistent with DB AOD over other regions. Furthermore, compared to MODIS DB, the spatial differences between POSP AOD and MODIS DT are smaller. In general, the results indicate a high degree of agreement between POSP and MODIS AOD, with differences predominantly within the (-0.2, 0.2) range." (LR 424-428)

In recent years, the global ground-based observation network has expanded significantly, improving coverage in many areas. However, ground-based observations remain sparse in remote and inaccessible regions. Given the current distribution of ground-based observation sites, it remains challenging to determine which aerosol product achieves the highest accuracy globally compared to others.

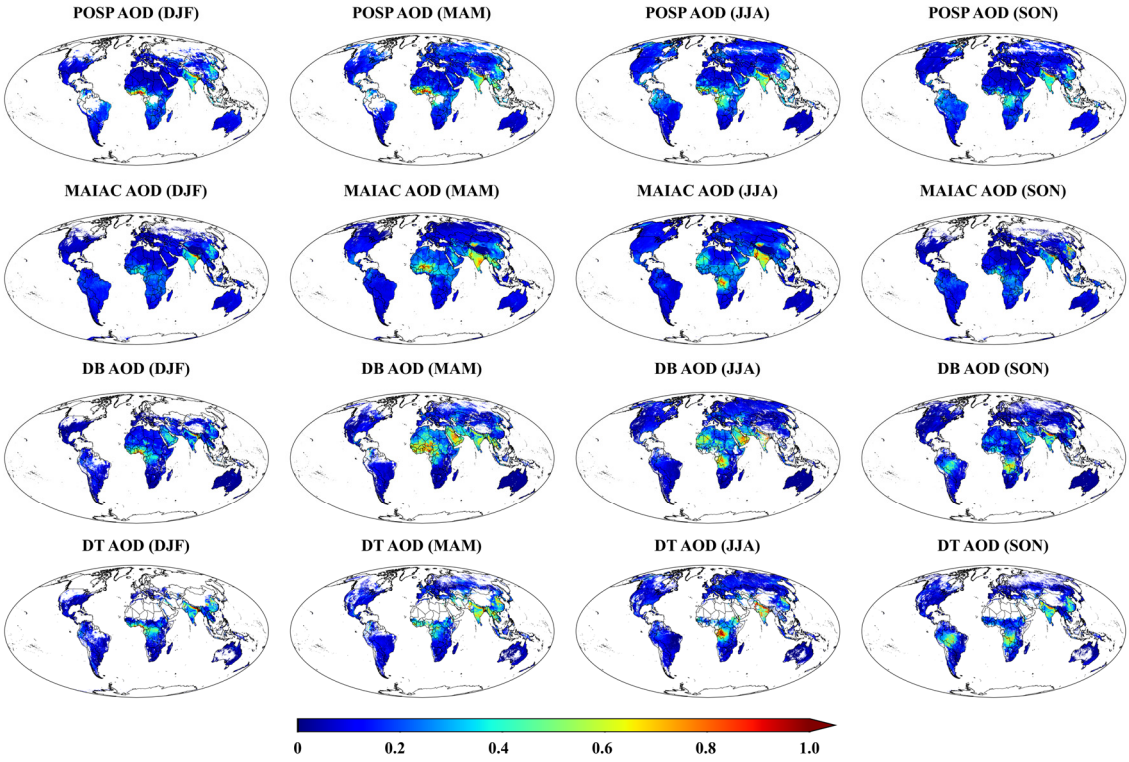

Figure 14: Maps of the seasonally averaged AOD derived from POSP, MODIS MAIAC, MODIS DB and MODIS DT, for the winter (DJF: December–January–February), spring (MAM: March–April-May,) summer (JJA: June–July–August), and autumn (SON: September–October–November).

This study performs retrievals based on a fixed aerosol model, which may lead to significant discrepancies between the assumed and actual aerosol models. Li et al. (2018) have quantitatively described the impact of aerosol model error on retrieval accuracy through simulation experiments. They applied the optimal estimation theory and calculated the degree of freedom for signal (DFS) available for aerosol retrieval parameters to quantify their information content (Frankenberg et al., 2012; Hasekamp and Landgraf, 2005). This method has been widely used to assess the theoretical retrieval capability of sensors.

Here, the aerosol model errors correspond with the combination of 6 predefined aerosol parameters: $\{r_{eff}^{f}$, v_{eff}^{f}, r_{eff}^{c}, v_{eff}^{c}, m_i^{f}, $m_i^{c}\}$, which are all assumed to change from 5% to 100% by a step of 5% with the constant measurement error, as well as the constant a priori errors of m_i^{f} and m_i^{c}. r_{eff}^{f} and r_{eff}^{c} represent the effective radius of fine- and coarse- mode aerosol, respectively. v_{eff}^{f} and v_{eff}^{c} represent the effective variance of fine- and coarse-mode aerosol, respectively. m_i^{f} and m_i^{c} represent the refractive index of fine- and coarse-mode aerosol, respectively. It is evident that as the aerosol model error increases, DFS decreases linearly, indicating that the retrieval uncertainty correspondingly increases.

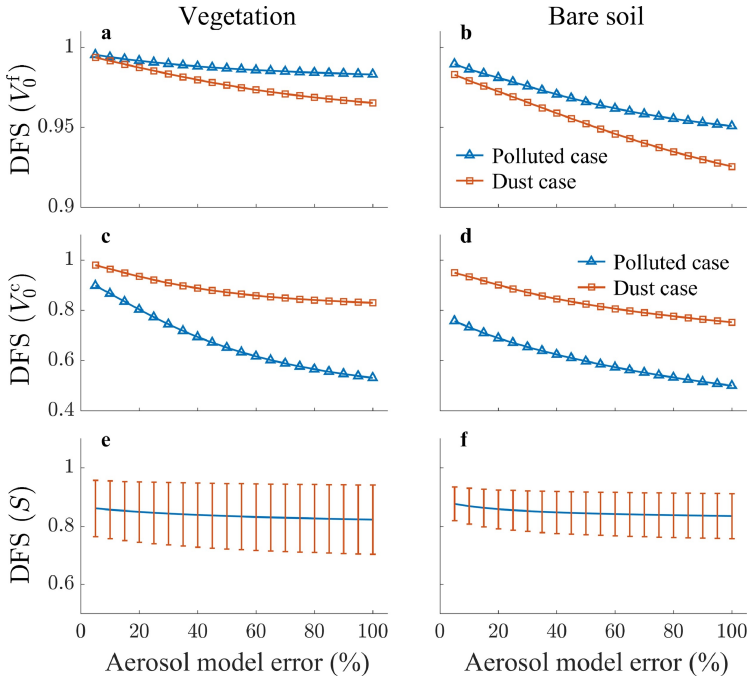

Fig. R1. Same as Fig. 11 but as a function of the aerosol model errors from 5% to 100% by a step of 5% with AOD=0.6.

We have added descriptions in the relevant sections regarding the impact of aerosol model error on retrieval accuracy.

"The probability density functions of differences (POSP-AERONET) are presented in Figure 2 (B). The results show that the POSP algorithm underestimates the AOD as aerosol loading increases. For low AOD (AOD < 0.2), POSP's bias is 0.01. For moderate AOD (0.2 ≤ AOD ≤ 0.7), POSP's bias increases to -0.03, and for high AOD (AOD > 0.7), POSP's bias further increases to -0.04. These biases may be attributed to the increasing aerosol model error. As AOD increases, the impact of discrepancies between the assumed aerosol model and the actual aerosol model is amplified, leading to an increase in retrieval uncertainty (Hou et al., 2018; Li et al., 2018)." (LR 218-223)

"On the other hand, in heavily polluted regions such as northern India, central and western Africa, and

central South America, POSP AOD shows high consistency with AERONET AOD, although the GCOS fraction is lower. This is because a fixed aerosol model is used to improve the stability of the inversion, which, however, may not accurately represent the actual aerosol types. Such discrepancies introduce greater uncertainties in the retrieval as the aerosol loading increases. Thus, using a fixed aerosol model inevitably affects the retrieval accuracy (Levy et al., 2013). This is one of the inherent challenges of aerosol retrieval using single-angle observations, and we aim to address this issue in future algorithm improvements." (LR 283-288)

GC3: Lines 302-304: The explanation for lower AOD accuracy in urban areas remains overly generalized ("complex surface and diverse pollution components"), lacking quantitative analysis (e.g., interference from urban surface reflectance anisotropy). Enhanced discussion on separating urban surface reflectance from aerosol signals is recommended.

Response to GC3: Thank you very much for pointing this out. Your comment is extremely valuable for improving the quality of our manuscript. We acknowledge that our analysis lacked a detailed discussion on the impact of urban surface reflectance anisotropy on aerosol retrievals. Therefore, we have now included a comprehensive discussion on this aspect, as detailed below.

"To further explore the impact of urban surface reflectance anisotropy on aerosol retrieval, synthetic experiments have been made. Following the detailed description of the spectral reconstruction of BRDF kernel coefficients in Section 2.1, here the BRDF kernel coefficients are filtered further for urban LC using the global IGBP classification product MCD12C1 (The MCD12C1 product was resampled to match the spatial resolution of the BRDF results). The number of BRDF kernel coefficients obtained over urban LC is quite large, making it impractical to compute TOA reflectance under different observation geometries and aerosol conditions for each individual case. To simplify the computation while retaining the representativeness of BRDF kernel coefficients over urban areas, we applied the K-means clustering method to extract BRDF kernel coefficients representative of urban areas in 2022 (tests showed that seven clusters are sufficient to represent the urban BRDF kernel coefficients). The results are presented in Table 3.

To evaluate the effect of ignoring surface directional characteristics over urban areas on the retrieved aerosol properties, the non-Lambertian radiative transfer model (RTM) and Lambertian RTM are used for creating synthetic TOA reflectances (ρ') and AOD retrieval results, respectively. In the retrieval process, the Lambertian RTM is used to calculate the TOA reflectance (ρ^*). The AOD corresponding to the best match between ρ^* and ρ' is taken as the retrieval result. By comparing the retrieval bias, the effect of ignoring surface anisotropy on AOD retrieval over urban areas was assessed.

The calculation of TOA reflectance requires consideration of three aspects: For the aerosol properties, to simulate aerosol conditions over urban areas, we used a mixture of continental and polluted aerosol types in equal proportions (Omar et al., 2009). And AOD was set to range from 0 to 1.5. Furthermore, in order to reduce the influence of errors introduced by aerosol model uncertainty, the aerosol model used in the retrieval is the same as that used in the creation of the synthetic dataset. For the surface reflectance, we used the seven representative BRDF kernel coefficients derived from the above clustering process. When calculating TOA reflectance using the non-Lambertian RTM, all three BRDF kernel coefficients from Table 3 are used to estimate the surface reflectance. In contrast, when using the Lambertian RTM, only the isotropic kernel coefficient from Table 3 is used as the surface reflectance. For the observation

geometries, the solar zenith angle, viewing zenith angle, and relative azimuth angle were set to range from 10° to 70°, 0° to 60°, and 0° to 360°, respectively. The observation geometry and AOD were both randomly sampled following a Gaussian distribution. To account for real-world observational conditions, we introduced random errors to the simulated reflectances consistent with calibration accuracy.

Figures 8 and 9 show polar diagrams of the surface reflectances, calculated using the MODIS BRDF model (Eqs. S1 to S9, with the solar zenith angle set at 30°), for each of the seven LC for urban types, as well as the scattering angle. These calculations were made for wavelengths used in the POSP retrieval algorithm, i.e., at 443 nm (Fig. 8) and 490 nm (Fig. 9). The simulations show that the surface reflectance increases significantly for viewing zenith angles larger than approximately 75°. In the retrieval algorithm, this issue is avoided by restricting the viewing zenith angles to less than 60°. Furthermore, surface reflectance increases substantially when the viewing zenith angle approaches the solar zenith angle, corresponding to the maximum scattering angle. This explains the high uncertainty over urban areas at large scattering angles discussed in Section 5.1.2.

Table 3 BRDF kernel coefficients statistics for different urban types.

Kernal name	Band (nm)	Type 1	Type 2	Type 3	Type 4	Type 5	Type 6	Type 7
Isotropic	443	0.068	0.044	0.053	0.104	0.076	0.049	0.127
	490	0.083	0.055	0.065	0.123	0.091	0.060	0.150
volumetric	443	0.017	0.021	0.017	0.028	0.041	0.036	0.058
	490	0.021	0.024	0.022	0.033	0.048	0.042	0.067
geometric-optical	443	0.016	0.010	0.011	0.023	0.014	0.007	0.020
	490	0.020	0.013	0.013	0.027	0.017	0.009	0.023

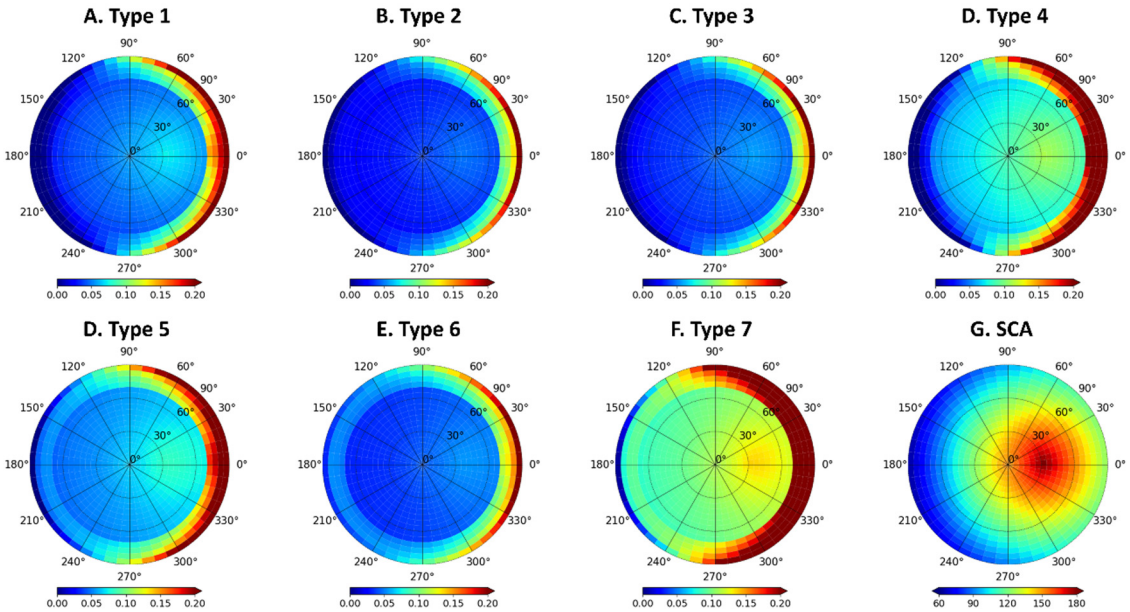

Figure 1: Polar diagrams of the BRDF distribution for the 7 types of clustered results. (A)-(F) The result of surface reflectance at 443 nm, and (G) The scattering angle plot. In this polar plot, the radius denotes a change in viewing zenith angle from 0° to 90°, and the polar angle represents a change in relative azimuth angle from 0° to 360°. The simulations are performed for a solar zenith angle of 30°. The colors in (A)–(F) and (G) represent surface reflectance and scattering angle magnitude, respectively.

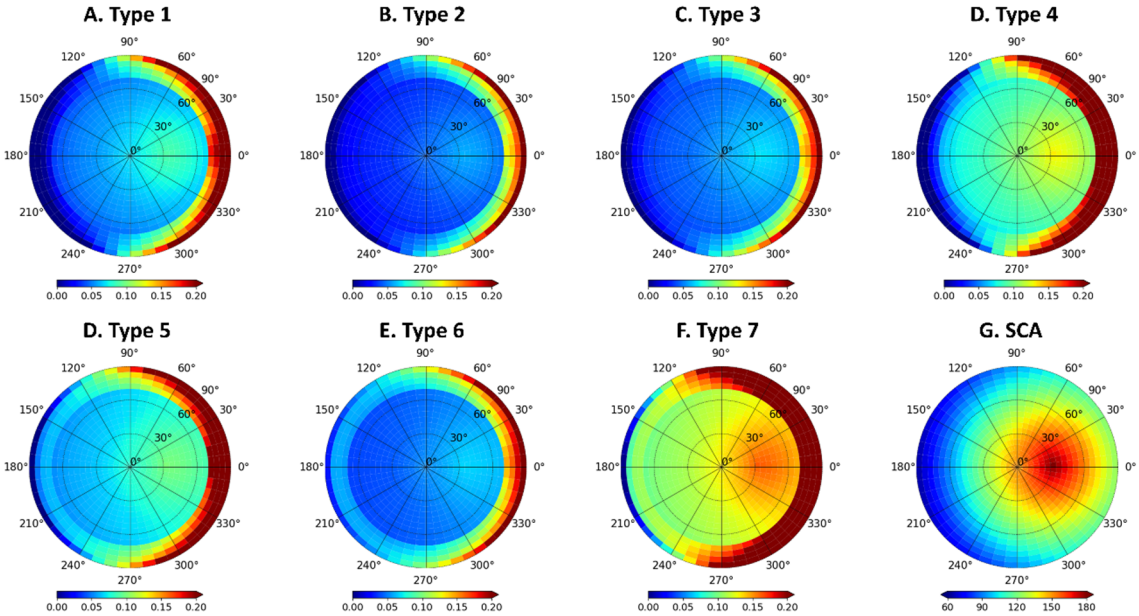

Figure 2: As Figure 8, but for a wavelength of 490 nm.

Figures 10 and S7 show the AOD bias as a function of scattering angle for 7 different surface types to illustrate how retrieval errors caused by neglecting surface anisotropy vary with scattering angle and aerosol loading, respectively. Because of the overestimation of the simulated reflectance using the Lambertian forward radiative transfer model, the retrieved AOD is underestimated. For types 4 and 7, which have the highest reflectance, the AOD underestimation is most pronounced, confirming that the higher the surface reflectance, the greater the impact of ignoring surface anisotropy on retrieval accuracy. For types 2 and 3, which have the lowest reflectance surfaces, the retrieval error caused by neglecting surface anisotropy is nearly constant across different aerosol loadings (Figure S7), but slightly increases as the scattering angle increases. Overall, as AOD increases, the impact of ignoring surface anisotropy on retrievals diminishes, and as surface reflectance increases.

Therefore, for aerosol retrieval over urban areas, the effect of surface anisotropy on the retrieval result is non-negligible in regions with high surface reflectance.

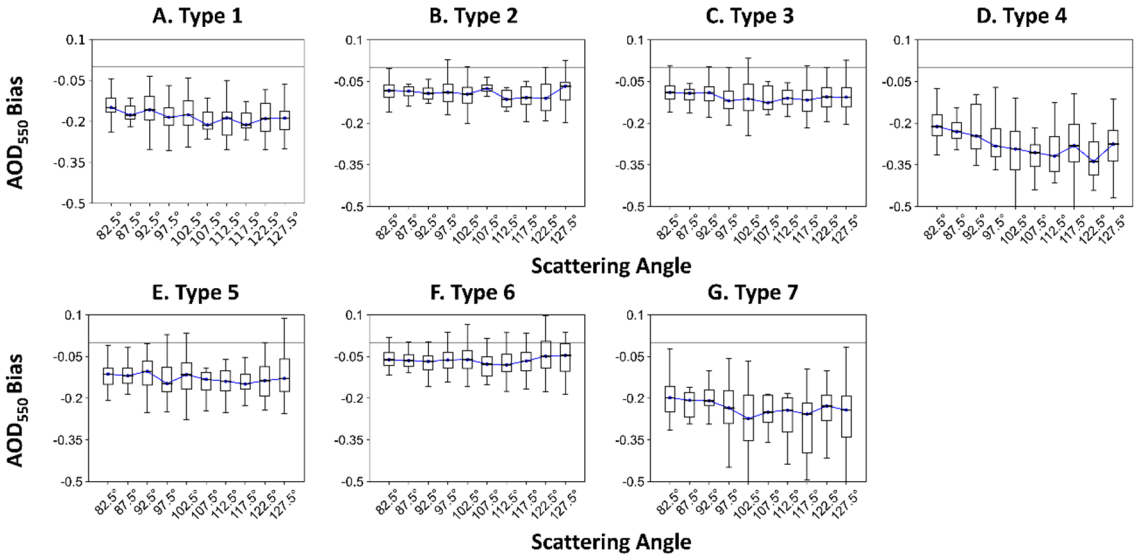

Figure 3: AOD bias as a function of scattering angle for different urban surface types.

" (LR 329-383)

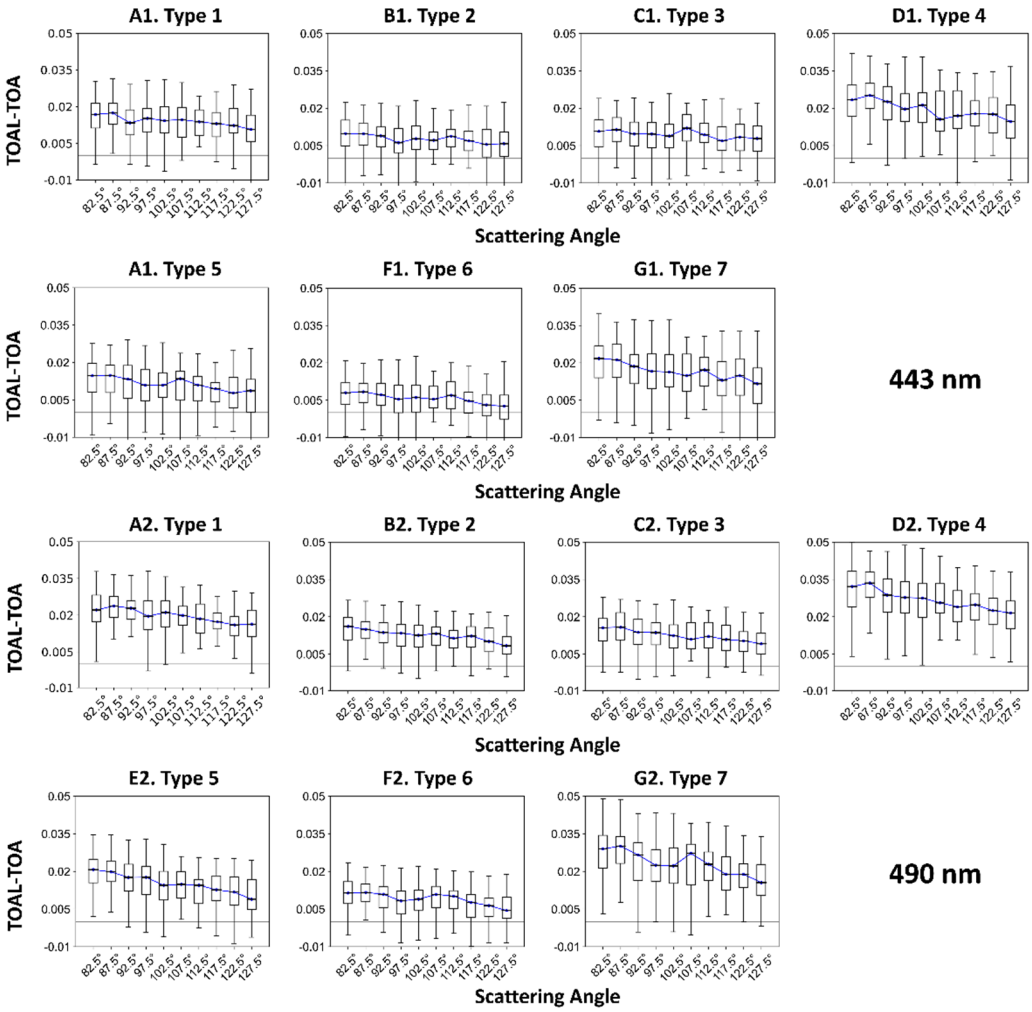

Figure S4: The boxplot of the differences for apparent reflectance between the results calculated based on the Lambertian forward radiative transfer model (TOAL) and the non-Lambertian forward radiative transfer model (TOA). The upper panel shows the differences as a function of AOD, while the lower panel presents the differences as a function of the scattering angle.

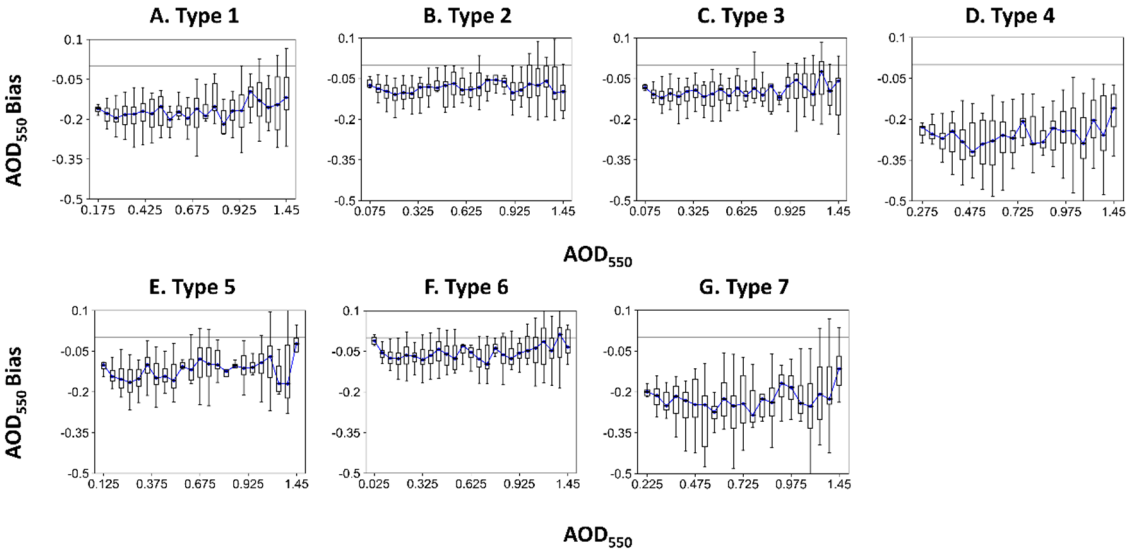

Figure S5: AOD bias as a function of aerosol loading for different urban surface types.

GC4: Line 246:"Other LC types which are not shown in Fig.4 are presented in Fig. S1." Figs. S1-S9 need to be found in the supplementary document. It is recommended to describe clearly in the manuscript.

Response to GC4: Thank you for these comments. We have revised the relevant sections to make the explanation as clear as possible.

GC5: Some grammatical inconsistencies exist. Comprehensive language polishing is advised to ensure proper tense usage and grammatical consistency throughout the manuscript.

Response to GC5: Thank you for these comments. We have substantially revised the MS. We have invited Professor Gerrit de Leeuw, an expert in the field of aerosol remote sensing, to revise our manuscript for grammatical errors and further improve the logic and organization. Furthermore, the manuscript has been carefully read and where necessary, unclear text has been re-formulated.

Citation: https://doi.org/10.5194/egusphere-2025-91-RC1

References:

Chu, D. A., Kaufman, Y. J., Ichoku, C., Remer, L. A., Tanré, D., and Holben, B. N.: Validation of MODIS aerosol optical depth retrieval over land, Geophysical Research Letters, 29, https://doi.org/10.1029/2001GL013205, 2002.

Frankenberg, C., Hasekamp, O., O'Dell, C., Sanghavi, S., Butz, A., and Worden, J.: Aerosol information content analysis of multi-angle high spectral resolution measurements and its benefit for high accuracy greenhouse gas retrievals, Atmospheric Measurement Techniques, 5, 1809–1821, 2012.

Frey, R. A., Ackerman, S. A., Liu, Y., Strabala, K. I., Zhang, H., Key, J. R., and Wang, X.: Cloud detection with MODIS. Part I: Improvements in the MODIS cloud mask for collection 5, Journal of Atmospheric and Oceanic Technology, 25, 1057–1072, https://doi.org/10.1175/2008JTECHA1052.1, 2008.

Hasekamp, O. P. and Landgraf, J.: Retrieval of aerosol properties over the ocean from multispectral single-viewing-angle measurements of intensity and polarization: Retrieval approach, information

content, and sensitivity study, Journal of Geophysical Research: Atmospheres, 110, 2005.

Hou, W., Li, Z., Wang, J., Xu, X., Goloub, P., and Qie, L.: Improving Remote Sensing of Aerosol Microphysical Properties by Near-Infrared Polarimetric Measurements Over Vegetated Land: Information Content Analysis, Journal of Geophysical Research: Atmospheres, 123, 2215–2243, 2018.

Kassianov, E. I. and Ovtchinnikov, M.: On reflectance ratios and aerosol optical depth retrieval in the presence of cumulus clouds, Geophysical Research Letters, 35, https://doi.org/10.1029/2008GL033231, 2008.

Levy, R. C., Mattoo, S., Munchak, L. A., Remer, L. A., Sayer, A. M., Patadia, F., and Hsu, N. C.: The Collection 6 MODIS aerosol products over land and ocean, Atmos. Meas. Tech., 6, 2989–3034, https://doi.org/10.5194/amt-6-2989-2013, 2013.

Li, Z., Hou, W., Hong, J., Zheng, F., Luo, D., Wang, J., Gu, X., and Qiao, Y.: Directional Polarimetric Camera (DPC): Monitoring aerosol spectral optical properties over land from satellite observation, Journal of Quantitative Spectroscopy and Radiative Transfer, 218, 21–37, https://doi.org/10.1016/j.jqsrt.2018.07.003, 2018.

Martins, J. V., Tanré, D., Remer, L., Kaufman, Y., Mattoo, S., and Levy, R.: MODIS cloud screening for remote sensing of aerosols over oceans using spatial variability, Geophysical Research Letters, 29, MOD4-1, 2002.

Omar, A. H., Winker, D. M., Vaughan, M. A., Hu, Y., Trepte, C. R., Ferrare, R. A., Lee, K.-P., Hostetler, C. A., Kittaka, C., Rogers, R. R., Kuehn, R. E., and Liu, Z.: The CALIPSO Automated Aerosol Classification and Lidar Ratio Selection Algorithm, Journal of Atmospheric and Oceanic Technology, 26, 1994–2014, https://doi.org/10.1175/2009JTECHA1231.1, 2009.